
Learning to Affiliate: Mutual Centralized Learning for Few-shot Classification

Yang Liu¹, Weifeng Zhang², Chao Xiang¹, Tu Zheng³, Deng Cai^{1,4*}

¹State Key Lab of CAD&CG, College of Computer Science, Zhejiang University

² Institute of Artificial Intelligence, College of Computer Science, Zhejiang University

³Fabu Inc., Hangzhou, China

⁴ Alibaba-Zhejiang University Joint Institute of Frontier Technologies

{lyng_95, zhangwf, chaoxiang}@zju.edu.cn, {zhengtuzju, dengcai}@gmail.com

Abstract

Few-shot learning (FSL) aims to learn a classifier that can be easily adapted to accommodate new tasks not seen during training, given only a few examples. To handle the limited-data problem in few-shot regimes, recent methods tend to collectively use a set of local features to densely represent an image instead of using a mixed global feature. They generally explore a unidirectional query-to-support paradigm in FSL, *e.g.*, find the nearest/optimal support feature for each query feature and aggregate these local matches for a joint classification. In this paper, we propose a new method *Mutual Centralized Learning* (MCL) to fully affiliate the two disjoint sets of dense features in a bidirectional paradigm. We associate each local feature with a particle that can bidirectionally random walk in a discrete feature space by the affiliations. To estimate the class probability, we propose the features' accessibility that measures the expected number of visits to the support features of that class in a Markov process. We relate our method to learning a centrality on an affiliation network and demonstrate its capability to be plugged in existing methods by highlighting centralized local features. Experiments show that our method achieves the state-of-the-art on both *miniImageNet* and *tieredImageNet*.

1 Introduction

Few-shot classification [19, 6, 9] aims to learn a classifier that can be readily adapted to novel classes given just a small number of labeled instances. To address this problem, a line of previous literature adopts metric-based methods [19, 16, 18] that learn to represent images with global embedding vectors in an appropriate feature space and use a distance metric to predict their labels.

Recent approaches [20, 7, 8] have demonstrated that the significant intra-class variations would inevitably drive the image-level embedding from the same category far apart in a given metric space under low-data regimes. In contrast, densely representative local features can provide transferrable information across categories that have shown promising performances in the few-shot scenario. Among those methods illustrated in Figure 1, Li *et al.*[7] find the nearest neighbor support feature for each query feature and accumulates all the local matches in a Naive-Bayes way to represent an image-to-class similarity; Lifchitz *et al.*[8] propose to make predictions with each local feature and average their output probabilities; Zhang *et al.*[20] use the earth mover distance to compare the complex structured representations composed of local features. They generally use the distances/similarities between two sets of dense features and perform classifications in a query-to-support paradigm by either aggregating these local matches [7, 8] or introducing the optimal matching flows [20].

*Deng Cai is the corresponding author

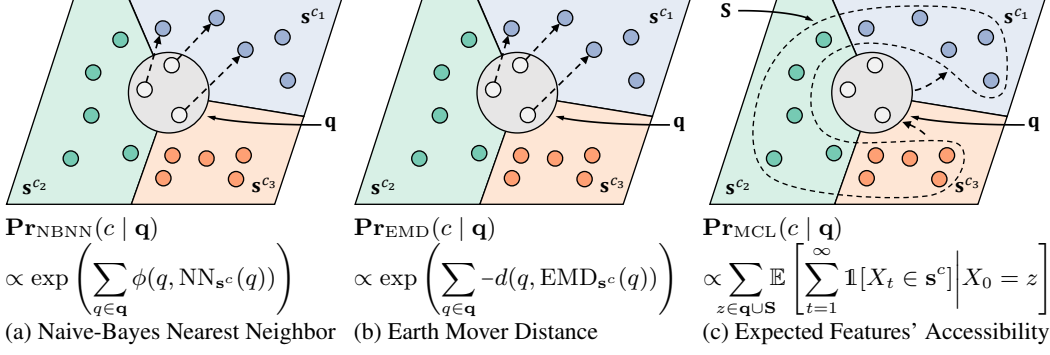


Figure 1: Comparisons of three methods in the 3-way 1-shot scenario where each image contains several dense features associated with particles of the same color. (a) NBNN [7] accumulates local similarities $\phi(\cdot, \cdot)$ between all query features and their nearest support features in a Naive-Bayes way as an image-to-class similarity; (b) EMD [20] finds the optimal matching flow that have the minimum distance cost $d(\cdot, \cdot)$ to represent the image-to-class distance; (c) We use the features’ accessibility (*i.e.*, the expected number of visits to support features of each class) in a bidirectional Markov random walk $\{X_t\}$ to measure the image-to-class relevance. A major difference is that we consider the mutual affiliations between dense features instead of following the unidirectional query-to-support paradigm.

In this work, we consider the extra support-to-query relation as a complement to fully affiliate two disjoint sets of dense features. The potential of mutual affiliations stems from the intuition that, except for using query features to find related support features, it is also plausible to estimate the relevance of query features according to the support features. To achieve this, we use the local similarity matrix as a basis to formulate the directional query-to-support and support-to-query affiliation matrices. We associate each local feature with a particle that could bidirectionally random walk in a discrete feature space by the mutual affiliations. We estimate the prediction probability for each class by the features’ accessibility (the expected number of visits to support features of that class) in a time-homogeneous Markov process. The motivation behind our method is that support features sharing the same class label with the query image would be frequently visited by their mutual closeness.

The contributions are as follows: (1) We consider the mutual affiliations between the query and support features instead of following the unidirectional query-to-support paradigm in FSL. (2) We propose to use the features’ accessibility that can directly estimate the prediction probability with dense features. (3) We draw connections to the single-mode eigenvector centrality of an affiliation network and further consider its variant Katz centrality [5] in graph theory. We find empirically that the choice of attenuation in Katz centrality is vital, as the strength of affiliations between two local features should devalue over long paths. (4) The underlying centrality investigated in this work can be plugged in existing methods like MatchingNet [19], ProtoNet [16] and RelationNet [18] by highlighting centralized local features before their mixed feature representations.

2 Method

2.1 Problem Formulation

In each episode for a N -way K -shot few-shot classification, we construct a support set \mathcal{S} with cardinal $N \times K$ that contains K different samples per class. There are several query images \mathcal{Q} that need to be classified to one of the support class in each episode. Both \mathcal{S} and \mathcal{Q} are sampled from labeled dataset $\mathcal{D}_{\text{train}}$ during training and the model is updated on this small sampled episode by minimizing classification loss on \mathcal{Q} . The generalization performance is measured by sampling similar \mathcal{S} and \mathcal{Q} episodically from test dataset $\mathcal{D}_{\text{test}}$ during the evaluation. We follow the recent dense feature based methods to learn M number of channel-dimensional features $f_{\theta}(x) \in \mathbb{R}^{C \times M}$ to represent local characteristics for each image x . We use $\mathbf{q} = \{q_1, \dots, q_M\}$ to represent the set of dense features from a query image and simply use the K -shot averaged features $\mathbf{s}^c = \{s_1^c, \dots, s_M^c\}$ to represent the set of dense features from support class c . The bold font of $\{\mathbf{q}, \mathbf{s}\}$ indicates a set of dense features while normal font $\{q, s\}$ indicates a single channel-dimensional feature vector. We use $\mathbf{S} = \bigcup_{c \in \mathcal{C}} \mathbf{s}^c$ to represent the union of features from all supporting classes.

2.2 Learning Mutual Affiliations through Bidirectional Random Walks

Our goal is to formulate and study an algorithm to find the label of a query image in a few-shot classification task, given dense query features \mathbf{q} and the union set \mathbf{S} of support features from all the classes. For simplicity of exposition, we denote $|\mathbf{q}|, |\mathbf{S}|$ as the cardinality of sets \mathbf{q} and \mathbf{S} respectively.

We start by defining local similarities between the two disjoint sets of dense features \mathbf{q}, \mathbf{S} following [7, 20, 8]. To be specific, given vectors v_1 and v_2 from the two feature sets respectively, we use the *scaled cosine similarity* $\phi_\gamma(v_1, v_2) = \gamma \langle v_1 / \|v_1\|, v_2 / \|v_2\| \rangle$ to measure their closeness where $\langle \cdot, \cdot \rangle$ denotes the Frobenius inner product and $\gamma \in \mathbb{R}^+$ is a scaling parameter.

Following the query-to-support convention in previous work, we affiliate each query feature q to support features $s \in \mathbf{S}$ with a random walk probability $p_{sq} = \exp(\phi_\gamma(s, q)) / \sum_{s' \in \mathbf{S}} \exp(\phi_\gamma(s', q))$ on the discrete feature space based on the relative closeness. The query-to-support probability matrix $\mathbf{P}_{\mathbf{S}\mathbf{q}} = (p_{sq})_{s \in \mathbf{S}, q \in \mathbf{q}}$ that indicates the probabilities for each $q \in \mathbf{q}$ random walking to $s \in \mathbf{S}$ can be formulated by

$$\mathbf{P}_{\mathbf{S}\mathbf{q}} = \Phi_\gamma \mathbf{D}^{-1} \quad (1)$$

where $\Phi_\gamma \in \mathbb{R}^{|\mathbf{S}| \times |\mathbf{q}|}$ is the exponential scaled similarity matrix with element entry $[\Phi_\gamma]_{sq} = \exp(\phi_\gamma(s, q))$. \mathbf{D} is a diagonal matrix with its (j, j) -value to be the sum of the j -th column of Φ_γ .

Unlike existing methods that simply consider the query-to-support matches in a unidirectional paradigm, we introduce an extra support-to-query relation as a complement to fully affiliate these two feature sets. Formally, we affiliate support feature s to query features $q \in \mathbf{q}$ by a similar random walk probability $p_{qs} = \exp(\phi_\tau(q, s)) / \sum_{q' \in \mathbf{q}} \exp(\phi_\tau(q', s))$. The analogous support-to-query probability matrix $\mathbf{P}_{\mathbf{q}\mathbf{S}} = (p_{qs})_{q \in \mathbf{q}, s \in \mathbf{S}}$ is given by

$$\mathbf{P}_{\mathbf{q}\mathbf{S}} = \Phi_\tau \mathbf{W}^{-1} \quad (2)$$

where $\Phi_\tau \in \mathbb{R}^{|\mathbf{q}| \times |\mathbf{S}|}$ and $[\Phi_\tau]_{qs} = \exp(\phi_\tau(q, s))$. \mathbf{W} is the similar diagonal normalization matrix.

We consider a support feature random walks from \mathbf{S} to \mathbf{q} and then walks back to \mathbf{S} as bidirectional random walks starting from \mathbf{S} . The probable locations for each support feature appearing at \mathbf{S} after walking and walking back are given by each column of probability matrix $\mathbb{R}^{|\mathbf{S}| \times |\mathbf{S}|} \ni \Psi_{\mathbf{S}} = \mathbf{P}_{\mathbf{S}\mathbf{q}} \mathbf{P}_{\mathbf{q}\mathbf{S}}$. By analogy, query features could also random walk from \mathbf{q} to \mathbf{S} and then walk back to appear at \mathbf{q} with a similar probability matrix $\mathbb{R}^{|\mathbf{q}| \times |\mathbf{q}|} \ni \Psi_{\mathbf{q}} = \mathbf{P}_{\mathbf{q}\mathbf{S}} \mathbf{P}_{\mathbf{S}\mathbf{q}}$.

Although the local similarity matrices Φ_γ and Φ_τ would be symmetric if we ignore their different scaling parameters γ and τ , the probability matrices $\mathbf{P}_{\mathbf{q}\mathbf{S}}$ and $\mathbf{P}_{\mathbf{S}\mathbf{q}}$ are both column-normalized and thus directional. Existing methods generally follow a *unidirectional* query-to-support paradigm by applying different metrics on $\mathbf{P}_{\mathbf{S}\mathbf{q}}$. For example, DN4 [7] accumulates similarities of each $q \in \mathbf{q}$ to their nearest neighboring $s \in \mathbf{S}$ based on $\mathbf{P}_{\mathbf{S}\mathbf{q}}$; DeepEMD [20] finds optimal matching flows between \mathbf{q} and \mathbf{S} according to $\mathbf{P}_{\mathbf{S}\mathbf{q}}$; Lifchitz [8] directly averages $\mathbf{P}_{\mathbf{S}\mathbf{q}}$ by \mathbf{q} . Unlike them, we introduce the extra support-to-query $\mathbf{P}_{\mathbf{q}\mathbf{S}}$ as a complement to learn their mutual affiliations through which similar characteristics are likely to be associated with each other by their mutual closeness.

2.3 Estimating Class Labels by the Long-term Features' Accessibility

We attack the classification problem based on the bidirectional random walks that encodes the mutual affiliations between the two dense feature sets \mathbf{q}, \mathbf{S} . The motivation of our method is straightforward: support features would be frequently visited in the long term of bidirectional random walks if they shared the same class label with the query image. In other words, support class that owns most querying characteristics would be the predicted class of the query image due to their mutual closeness.

To formulate it, we associate each local feature with a particle z that is allowed to bidirectionally random walk in a discrete feature space $\mathbf{z} = \mathbf{q} \cup \mathbf{S}$ and assume these discrete random walks time-homogeneous in a Markov process $\{X_t\}$. Formally, the probability from z_j to z_i is

$$\Pr(X_{t+1} = z_i | X_t = z_j) = \begin{cases} \exp(\phi_\gamma(z_i, z_j)) / \sum_{s \in \mathbf{S}} \exp(\phi_\gamma(s, z_j)) & z_i \in \mathbf{S}, z_j \in \mathbf{q} \\ \exp(\phi_\tau(z_i, z_j)) / \sum_{q \in \mathbf{q}} \exp(\phi_\tau(q, z_j)) & z_i \in \mathbf{q}, z_j \in \mathbf{S} \\ 0 & \text{otherwise} \end{cases} \quad (3)$$

and the probability for all particles in the discrete feature space is given by the entry of

$$\mathbf{P} = \begin{pmatrix} \mathbf{0} & \mathbf{P}_{\mathbf{S}\mathbf{q}} \\ \mathbf{P}_{\mathbf{q}\mathbf{S}} & \mathbf{0} \end{pmatrix} \quad (4)$$

where \mathbf{P} is an anti-diagonal matrix that consists of the column-normalized sub-matrices $\mathbf{P}_{\mathbf{S}\mathbf{q}}$ and $\mathbf{P}_{\mathbf{q}\mathbf{S}}$ defined in Eqn.(1) and Eqn.(2) respectively. The subscript of sub-matrices serves both as the matrix size and as an indication for the particle with which it is associated. For example, $\mathbf{P}_{\mathbf{S}\mathbf{q}}$ is of size $|\mathbf{S}| \times |\mathbf{q}|$ and indicates the probabilities from query features \mathbf{q} to support features \mathbf{S} .

It can be proved (in Appendix B) that the Markov chain with anti-diagonal transition matrix \mathbf{P} is periodic and its stationary distributions are of period 2:

$$\lim_{t \rightarrow \infty} \mathbf{P}^{2t} = \begin{pmatrix} \boldsymbol{\pi}(\mathbf{S}) \mathbf{e}_{|\mathbf{S}|}^T & \mathbf{0} \\ \mathbf{0} & \boldsymbol{\pi}(\mathbf{q}) \mathbf{e}_{|\mathbf{q}|}^T \end{pmatrix} \quad \lim_{t \rightarrow \infty} \mathbf{P}^{2t-1} = \begin{pmatrix} \mathbf{0} & \boldsymbol{\pi}(\mathbf{S}) \mathbf{e}_{|\mathbf{q}|}^T \\ \boldsymbol{\pi}(\mathbf{q}) \mathbf{e}_{|\mathbf{S}|}^T & \mathbf{0} \end{pmatrix} \quad (5)$$

where $\boldsymbol{\pi}(\mathbf{S}) \in \mathbb{R}^{|\mathbf{S}|}$, $\boldsymbol{\pi}(\mathbf{q}) \in \mathbb{R}^{|\mathbf{q}|}$ are the stationary distributions of aforementioned bidirectional random walks in Section 2.2 with equations $\boldsymbol{\pi}(\mathbf{S}) = \boldsymbol{\Psi}_{\mathbf{S}} \boldsymbol{\pi}(\mathbf{S})$ and $\boldsymbol{\pi}(\mathbf{q}) = \boldsymbol{\Psi}_{\mathbf{q}} \boldsymbol{\pi}(\mathbf{q})$ respectively. $\mathbf{e}_{|\cdot|}$ is a vector of ones with different length indicated by its subscript.

To perform classification, we first assume particles uniformly distributed in the discrete finite space $\mathbf{z} = \mathbf{q} \cup \mathbf{S}$. Then, we use the expected number of visits from all particles $z \in \mathbf{z}$ to support features $\mathbf{s}^c \subset \mathbf{S}$ of class c in the long term of bidirectional random walks $\{X_t\}$ as a measure:

$$\begin{aligned} \mathbf{Pr}(\tilde{y} = c) &\propto \lim_{t \rightarrow \infty} \sum_{z \in \mathbf{z}} \mathbb{E} \left[\sum_{k=1}^t \mathbb{1}[X_k \in \mathbf{s}^c] \middle| X_0 = z \right] \\ &= \lim_{t \rightarrow \infty} \frac{1}{t} \sum_{k=1}^t \left[\frac{1}{|\mathbf{S}| + |\mathbf{q}|} \sum_{s \in \mathbf{s}^c} \left(\sum_{s' \in \mathbf{S}} [\mathbf{P}^{2k}]_{ss'} + \sum_{q \in \mathbf{q}} [\mathbf{P}^{2k-1}]_{sq} \right) \right] \\ &= \frac{1}{|\mathbf{S}| + |\mathbf{q}|} \sum_{s \in \mathbf{s}^c} \left(\sum_{s' \in \mathbf{S}} \left[\lim_{t \rightarrow \infty} \mathbf{P}^{2t} \right]_{ss'} + \sum_{q \in \mathbf{q}} \left[\lim_{t \rightarrow \infty} \mathbf{P}^{2t-1} \right]_{sq} \right) = \sum_{s \in \mathbf{s}^c} [\boldsymbol{\pi}(\mathbf{S})]_s \end{aligned} \quad (6)$$

where $\mathbb{1}[\cdot]$ is an indicator function that equals 1 if its argument is true and zero otherwise. $[\cdot]_{ij}$ indicates the entry of the matrix from particle j to particle i and $[\cdot]_i$ indicates the entry of the vector that associated to feature i .

It should be noted that we give the derivation when the Markov chain length t is even in the first equality of Eqn.(6) and prove that the odd t will reach the same result in Appendix D. The second equality is from the *absorbing* of the periodic Markov chain where the power of matrix get saturated to Eqn.(5) when the value of t increases. Since $\boldsymbol{\pi}(\mathbf{S})$ is the stationary distribution of column-stochastic $\boldsymbol{\Psi}_{\mathbf{S}}$ under the probability constraint $\mathbf{e}_{|\mathbf{S}|}^T \boldsymbol{\pi}(\mathbf{S}) = 1$, $\mathbf{Pr}(\tilde{y})$ is a valid distribution for class predictions.

2.4 Reinterpretation as a Graph Centrality

If we interpret the Markov transition matrix \mathbf{P} as an adjacency matrix $\{a_{v_1, v_2}\}$ of a directed bipartite graph $G := (V = \{\mathbf{q}, \mathbf{S}\}, E)$, we find that the accessibility of support features in the time-homogeneous bidirectional random walk would be equivalent to learning a *single-mode eigenvector centrality* on graph G . The bipartite graph is also called the *affiliation network* in social network analysis [1, 2, 3] that models two types of entities "actors" and "society" related by affiliation of the former in the latter. The concept of centrality in social network analysis is generally used to investigate the acquaintanceships among people that often stem from one or more shared affiliations.

To see this in graph theory, we start with a brief overview of the eigenvector centrality \mathbf{x} that reflects scores of vertexes for both $q \in \mathbf{q}$ and $s \in \mathbf{S}$ in the affiliation network with adjacency $\{a_{v_1, v_2}\}$:

$$\mathbf{x}_q = \frac{1}{\lambda} \sum_{v \in \mathbb{V}(q)} a_{q, v} \mathbf{x}_v = \frac{1}{\lambda} \sum_{v \in \mathbf{S}} a_{q, v} \mathbf{x}_v \quad \mathbf{x}_s = \frac{1}{\lambda} \sum_{v \in \mathbb{V}(s)} a_{s, v} \mathbf{x}_v = \frac{1}{\lambda} \sum_{v \in \mathbf{q}} a_{s, v} \mathbf{x}_v \quad (7)$$

where $\mathbb{V}(\cdot)$ is a set of neighbors for the given vertex and λ is a constant. With a small rearrangement, Eqn.(7) can be rewritten in vector notation with an eigenvector equation $\mathbf{P}\mathbf{x} = \lambda\mathbf{x}$. The additional requirement that all the entries of the eigenvector be non-negative implies (by the Perron–Frobenius theorem [11]) that only the greatest eigenvalue results in the desired centrality measure. For the adjacency matrix defined by the Markov transition matrix in our method, the largest eigenvalue λ of the column-stochastic matrix \mathbf{P} is 1.

Lemma 1. Assume G is the affiliation network of bipartite data $\{\mathbf{q}, \mathbf{S}\}$ with the adjacency matrix defined by the anti-diagonal Markov transition matrix \mathbf{P} in Eqn.(4). The single-mode eigenvector centrality $\hat{\mathbf{x}}_{\mathbf{S}} = \mathbf{x}_{\mathbf{S}} / \sum_{s \in \mathbf{S}} \mathbf{x}_s$ of vertex set \mathbf{S} is equivalent to the features' accessibility $\pi(\mathbf{S})$ on \mathbf{S} in a long term of time-homogeneous Markov process.

Single-mode centrality [3] is a special form of centrality that measures the extent to which nodes in one vertex set are relatively central only to other nodes in the same vertex set for bipartite graphs. For example, the single-mode eigenvector centrality for different s in \mathbf{S} is defined by $\hat{\mathbf{x}}_{\mathbf{S}} = \mathbf{x}_{\mathbf{S}} / \sum_{s \in \mathbf{S}} \mathbf{x}_s$. Lemma 1 (proved in Appendix C) shows that features' accessibility $\pi(\mathbf{S})$ in Eqn.(6) is equivalent to the single-mode eigenvector centrality of support set \mathbf{S} on bipartite data.

Based on this interpretation, it is straightforward to consider the attenuation (damping) factor α on the affiliation network motivated by the well-known Katz centrality, a well-known variant of eigenvector centrality in graph theory [5]. The features' accessibility of Markov bidirectional random walks with attenuation α for few-shot classifications is defined by

$$\begin{aligned} \Pr_{\text{Katz}}(\tilde{y} = c) &\propto \sum_{z \in \mathbf{z}} \mathbb{E} \left[\sum_{t=1}^{\infty} \alpha^t \mathbf{1}[X_t \in \mathbf{s}^c] \middle| X_0 = z \right] \\ &= \frac{1}{\epsilon} \sum_{t=1}^{\infty} \sum_{s \in \mathbf{s}^c} \left(\sum_{s' \in \mathbf{S}} [\alpha^{2t} \mathbf{P}^{2t}]_{ss'} + \sum_{q \in \mathbf{q}} [\alpha^{2t-1} \mathbf{P}^{2t-1}]_{sq} \right) \end{aligned} \quad (8)$$

where $\epsilon = (|\mathbf{S}| + |\mathbf{q}|) \sum_{t=1}^{\infty} \alpha^t = (|\mathbf{S}| + |\mathbf{q}|) \alpha / (1 - \alpha)$ is a constant for a valid distribution.

Although we simply consider the single-mode centrality on \mathbf{S} for an end-to-end classification purpose, it is also beneficial to learn its conjugate centrality $\pi(\mathbf{q})$ for \mathbf{q} on the affiliation network. We will show that both centralities could serve as plug-and-play for finding centralized local characteristics in existing methods (hence the term Mutual Centralized Learning, MCL).

2.5 Mutual Centralized Learning

The algorithm of Mutual Centralized Learning (MCL) in Eqn.(6, 8) involves the computation of Markov stationary distribution $\pi(\mathbf{S})$ with equation $\pi(\mathbf{S}) = \Psi_{\mathbf{S}} \pi(\mathbf{S})$. Theoretically, the $\pi(\mathbf{S})$ is the eigenvector of $\Psi_{\mathbf{S}}$ with the eigenvalue 1 under a probability constraint $e_{|\mathbf{S}|}^T \pi(\mathbf{S}) = 1$.

The above constraints could lead to a solution of $\pi(\mathbf{S})$ by solving the overdetermined linear system

$$\begin{pmatrix} \Psi_{\mathbf{S}} - \mathbf{I} \\ e_{|\mathbf{S}|}^T \end{pmatrix} \pi(\mathbf{S}) = \begin{pmatrix} \mathbf{0} \\ 1 \end{pmatrix} \quad (9)$$

where \mathbf{I} is an identity matrix and $\mathbf{0}$ is a vector of zeros. Although we can solve it by various methods like pseudo-inverse or QR decomposition and back substitution, it is empirically found time-consuming as these operators are either numerically unstable or not paralleled well in modern deep-learning packages such as Pytorch [10].

To handle it, we present a fast solution by the graph centrality. We first use the closed-form solution in [5] to get the whole Katz centrality and then solve single-mode Katz centrality in Eqn.(8) by

$$\mathbf{x}^{\text{Katz}} = ((\mathbf{I} - \alpha \mathbf{P})^{-1} - \mathbf{I}) \mathbf{e} \quad (10)$$

$$\Pr_{\text{Katz}}(\tilde{y} = c) = \frac{\sum_{s \in \mathbf{s}^c} \mathbf{x}_s^{\text{Katz}}}{\sum_{s' \in \mathbf{S}} \mathbf{x}_{s'}^{\text{Katz}}} \quad (11)$$

where \mathbf{e} is vector of ones with length $|\mathbf{S}| + |\mathbf{q}|$. Since Katz centrality degrades to the eigenvector centrality when α approaches 1 (indicating no attenuation), we can obtain a fast approximation of Eqn.(6) with a large $\alpha = 0.999$:

$$\mathbf{x}^{\text{Eigen}} = \lim_{\alpha \rightarrow 1} ((\mathbf{I} - \alpha \mathbf{P})^{-1} - \mathbf{I}) \mathbf{e} \approx ((\mathbf{I} - 0.999 \mathbf{P})^{-1} - \mathbf{I}) \mathbf{e} \quad (12)$$

$$\Pr_{\text{MCL}}(\tilde{y} = c) = \frac{\sum_{s \in \mathbf{s}^c} \mathbf{x}_s^{\text{Eigen}}}{\sum_{s' \in \mathbf{S}} \mathbf{x}_{s'}^{\text{Eigen}}} \quad (13)$$

We found this approximation could achieve exactly the same performance as directly solving the overdetermined linear system in Eqn.(9) but is 4× faster throughout the experiments. We give the whole picture of proposed Mutual Centralized Learning with episode loss for few-shot classifications in Appendix A.

3 Related Work

Global Feature based Few-shot Learning. Traditional metric-based methods [19, 18, 16, 15] use compact feature vectors to represent images. They generally use the output from the last global average pooling layer of the embedding network and then perform classifications by different metrics. Among those methods, MatchingNet [19] trains a learnable nearest neighbor classifier with a deep neural network. Prototypical Network [16] takes the mean of each class as its corresponding prototype representation to learn a metric space. RelationNet [18] introduces an auxiliary non-linear metric to compute the similarity score between each query and support features. However, this global averaged representation could easily lose considerable local information especially under low-data regimes.

Dense Feature based Few-shot Learning. Another branch of metric-based methods focuses on learning image-to-image similarities based on the local features. Among them, Lifchitz *et al.*[8] proposes to make predictions for each local characteristic and average their output probabilities. DeepEMD [20] adopts the earth mover’s distance as a metric to compute a structural distance between dense features to determine the image relevance. DN4 [7] uses the top- k nearest neighbors between two dense features in a Naive-Bayes way to represent image-level similarities. Our MCL is also among the family of dense feature based frameworks. A major difference of our method is that we consider the mutual affiliations between two sets of dense features instead of simply using the query-to-support matches in a unidirectional paradigm.

Propagation based Few-shot Learning. Liu *et al.*[9] first introduced the well-known label spreading [21] to the transductive FSL that transfers information from labeled data to unlabeled one, and shows substantial improvements over inductive methods. In this paper, we demonstrate it also feasible to adopt propagation methods for the inductive FSL by treating the dense query features as numerous unlabeled data. Our method is also a special form of propagation methods that bidirectionally random walks in a discrete finite feature space. Differently, we consider the set of query and support features as bipartite data where the *self-reinforcements* (*i.e.*, query-to-query and support-to-support random walks) are avoided. As a result, each local feature is forced to randomly walk to the opposite set of features with their mutual affiliations.

4 Experiments

4.1 Experiment Setups

Datasets. We performed experiments on two FSL datasets *miniImageNet* [19] and *tieredImageNet* [12], both of which are subsets of ImageNet: (1) **miniImageNet** [19] contains 600 images per class over 100 classes. We followed the split proposed in [13] that takes 64, 16 and 20 classes for train/val/test respectively. (2) **tieredImageNet** [12] is much larger compared to *miniImageNet* with 608 classes and each class around 1,300 samples. These classes were grouped into 34 higher-level concepts and then partitioned into 20/6/8 disjoint sets for train/val/test to achieve a larger domain difference.

Backbone networks. We conduct experiments with both widely-used four layer convolutional **Conv-4** [19] and deep **ResNet-12** [17] backbones. All images in both query and support sets are cropped and resized to 84×84 before fed into the embedding network. As is commonly implemented in the state-of-the-art FSL literature, we adopt a pretraining stage for the deeper ResNet-12 before the episode meta-training while meta-train directly from the scratch for the simple Conv-4 backbone. The model is evaluated by sampling 10,000 episodes from test set.

Selections of hyper-parameters γ , τ and α . Parameters γ and τ in Eqn.(1,2) are selected by the best validation performances on the pre-trained backbone and will be discussed in the ablative analysis. We use $\alpha = 0.5$ for **MCL-Katz** in Eqn.(8) and use $\alpha = 0.999$ to fast approximate **MCL** in Eqn.(6).

Dense feature extractor $f_\theta(\cdot)$. For a fair comparison with the previous dense feature based methods [7, 20], we explore three dense feature extractors in our experiments: *VanillaFCN* simply treats the feature map output of fully convolutional network as dense features; *PyramidFCN* applies pyramid structures on top of FCN to extract dense features of different scales; *PyramidGrid* crops image into grid patches of different scales and encode each patch to a feature vector with embedding network. We present more details of mentioned dense feature extractors in Appendix E.

Table 1: Few-shot classification accuracy (%) on *miniImageNet* and *tieredImageNet* dataset with different backbones. \dagger indicates our reimplementations in the same setting for a fair comparison. We report DeepEMD $^\sharp$ [20] 5-shot results in without their episode-wise finetuning on the test dataset.

Method	Conv-4				ResNet-12				
	<i>miniImageNet</i>		<i>tieredImageNet</i>		<i>miniImageNet</i>		<i>tieredImageNet</i>		
	1-shot	5-shot	1-shot	5-shot	1-shot	5-shot	1-shot	5-shot	
<i>Global features</i>	DSN [15]	51.78	68.99	53.22	71.06	62.64	78.83	67.39	82.85
	MetaOptNet [6]	52.87	68.76	54.71	71.76	62.64	78.63	65.99	81.56
	RelationNet \dagger [18]	52.12	66.90	54.33	69.95	60.97	75.12	64.71	78.41
	RelationNet+MCL	54.37	70.57	57.68	74.46	61.70	75.53	65.93	80.27
	ProtoNet \dagger [16]	52.32	69.74	53.19	72.28	62.67	77.88	68.48	83.46
	ProtoNet+MCL	54.31	69.84	56.60	74.18	64.40	76.74	70.62	83.84
	MatchingNet \dagger [19]	53.96	69.88	56.19	74.05	62.70	80.93	69.92	85.79
<i>Dense features</i> (<i>VanillaFCN</i>)	MatchingNet+MCL	54.81	69.41	56.68	74.29	62.74	80.86	70.50	86.06
	DN4 \dagger [7]	54.66	71.26	56.86	72.16	64.84	77.74	69.60	83.41
	DeepEMD $^\sharp$ [20]	52.15	65.52	50.89	66.12	65.91	79.74	71.16	83.95
	Label Spreading	52.24	67.68	54.56	70.08	65.00	80.07	71.12	83.89
	MCL (ours)	55.38	69.17	57.63	72.62	66.23	81.79	71.76	85.68
	MCL-Katz (ours)	55.55	71.74	57.78	73.21	66.29	81.94	72.01	86.02
<i>Dense features</i> (<i>PyramidFCN</i>)	DN4 \dagger [7]	54.54	70.94	57.05	72.90	63.54	79.04	71.10	84.22
	DeepEMD $^\sharp$ [20]	50.67	64.94	51.26	65.64	66.27	79.78	70.76	84.20
	Label Spreading	53.38	68.69	55.21	71.22	65.71	75.78	71.00	78.01
	MCL (ours)	55.13	70.10	56.87	72.97	66.31	81.88	72.01	86.31
	MCL-Katz (ours)	55.77	71.24	57.44	73.27	66.37	81.96	72.13	86.32
<i>Dense features</i> (<i>PyramidGrid</i>)	DN4 \dagger [7]	57.17	70.91	56.71	70.92	67.86	80.08	71.29	82.60
	DeepEMD $^\sharp$ [20]	55.68	70.75	55.88	70.06	67.83	81.32	73.13	84.18
	Label Spreading	55.12	68.43	56.05	72.39	67.18	81.07	73.18	85.19
	MCL (ours)	57.50	73.03	57.57	73.81	68.42	83.18	73.62	86.29
	MCL-Katz (ours)	57.88	74.03	56.98	73.96	68.39	83.33	73.38	86.21

4.2 Few-shot Classification Results

Table 1 shows the few-shot classification accuracy on *miniImageNet* and *tieredImageNet* of proposed Mutual Centralized Learning (MCL) compared to both global feature [19, 15, 18, 16, 6] and dense feature [7, 20] based methods in previous literature. Besides these methods, we also exploit the well-known label spreading [21] in dense feature based FSL as a baseline.

Comparisons with global feature based methods. We first compare our method with a set of metric-based methods that utilize global features to represent images. These methods generally use a global averaged pooling layer at the end of the backbone to obtain a mixed representation and perform classifications by different metrics. To compare, we select representative methods in the literature: ProtoNet [16] with Euclidean distance, MatchingNet [19] with cosine distance and RelationNet [18] with a fully connected binary classifier. We show in Table 2 that MCL significantly outperforms them by a large margin benefited from the preserved local characteristics.

Comparisons with dense feature based methods. We conduct thorough experiments to compare with dense feature based methods by exploring various dense feature extractors in Table 1. It can be observed that our proposed mutual affiliations consistently outperforms the unidirectional query-to-support nearest matches in DN4 [7] and optimal matching flows in DeepEMD [20]. The relative improvement of MCL over DeepEMD is less impressive compared to the improvement over DN4. We speculate that the cross-reference attention mechanism in DeepEMD accounts for it as their bidirectional attention also encodes the mutual relevance between the query and support features. To validate it, we retrain and test the DeepEMD without their proposed attention and find the accuracy significantly drops $\sim 2\%$ (e.g., 63.57% for 1-shot *miniImageNet* with *VanillaFCN*), which to some extent supports our claim that the mutual affiliations are beneficial in FSL.

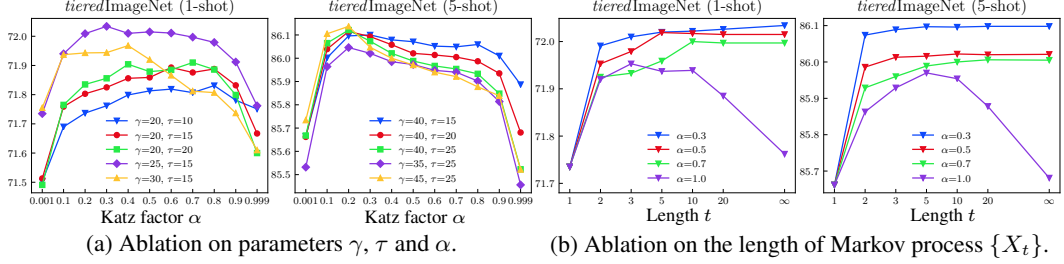


Figure 2: Ablative results of 5-way few-shot learning tasks on *tieredImageNet* with ResNet-12 and *VanillaFCN* feature extractor. (a) studies the influences from different choices of parameters. (b) compares performances between infinite length of Markov process and those from varying finite lengths.

	$f_\theta(\cdot)$	Metric	5-way	10-way
ProtoNet [16]		Euclidean	62.67	44.34
MatchingNet [19]		<i>cosine</i>	62.70	47.09
RelationNet [18]	<i>global</i>	<i>classifier</i>	60.97	43.95
Chen <i>et al.</i> [4]		<i>dot</i>	59.41	44.08
Chen <i>et al.</i> [4]		<i>cosine</i>	55.43	40.42
DN4 [7]		<i>cosine</i>	64.84	47.08
DC [8]		<i>cosine</i>	62.38	47.04
DeepEMD [20]	<i>dense</i>	EMD	65.91	49.66
MCL (ours)		<i>centrality</i>	66.23	49.80
MCL-Katz (ours)		<i>centrality</i>	66.29	50.07

Table 2: Comparison of different metric-based methods for 1-shot classification with ResNet-12 and *VanillaFCN* on *miniImageNet*.

	\mathbf{q}	\mathbf{s}	+MCL	<i>mini-</i>		<i>tiered-</i>	
			1-shot	5-shot	1-shot	5-shot	5-shot
ProtoNet [16]	✓		52.32	69.74	53.19	72.28	
		✓	53.74	69.61	55.36	73.17	
	✓	✓	53.97	69.74	56.60	74.18	
RelationNet [18]	✓		54.31	69.84	55.94	72.78	
		✓	52.12	66.90	54.33	69.95	
	✓	✓	53.25	66.79	54.46	70.71	
		✓	54.37	70.57	57.68	74.24	
	✓	✓	53.97	70.36	57.23	74.46	

Table 3: Ablation of MCL as plug-and-play that individually applied on query features \mathbf{q} and support features \mathbf{s} . The experiments are conducted with Conv-4 and *VanillaFCN* on *mini-/tieredImageNet*.

MCL as plug-and-play for centrality weighted pooling. Since the underlying centrality learned by MCL reveals the different importance of local features on an affiliation network, it is thus plausible to plug it into global feature based methods by replacing the native global average pooling with the centrality weighted pooling. We conduct experiments in Table 1 and find it could provide at most 0.9%, 3.4% and 4.5% performance gains for MatchingNet [19], ProtoNet [16] and RelationNet [18] respectively. We demonstrate in Table 3 that the improvements are also consistent if we individually apply the centrality weighted pooling on the query and support features.

4.3 Ablative Analysis

Different choices of scaling hyper-parameters γ and τ . We use two different hyper-parameters γ, τ in scaled cosine similarity matrices $\Phi_\gamma \in \mathbb{R}^{|S| \times |\mathbf{q}|}$ and $\Phi_\tau \in \mathbb{R}^{|\mathbf{q}| \times |S|}$. With the column-wise normalization in Eqn.(1,2), γ and τ can be interpreted as the reciprocal of temperatures in softmax-like probability. Generally, a large scaling parameter means a confident probability of a random walk that leads to a more concentrated centrality in the affiliation network. However, an extremely hard random walk probability (*e.g.*, one-hot probability when γ, τ approach infinity) would inevitably bias the episodic training due to the potential gradient explosion. In the experiments, we carefully select γ and τ by the validation performances of pretrained models and compare their different combinations in Figure 2(a). Since the cardinality $|S|$ is generally larger than $|\mathbf{q}|$, we empirically use a larger γ than τ in the experiments as we need a more confident probability in random walks from query features to the large union set of support features in which most of them could be task-irrelevant.

Influence of Katz attenuation factor α . Intuitively, the contributions of distant nodes should be penalized by attenuation in the long term of random walks. For a small value of α , the contribution given by paths longer than one rapidly declines, and thus the centrality is mainly influenced by short paths (mostly in-degrees). When α is large, long paths are devalued smoothly, and the centrality would be more influenced by endogenous topology. We show the ablative on α in Figure 2(a)

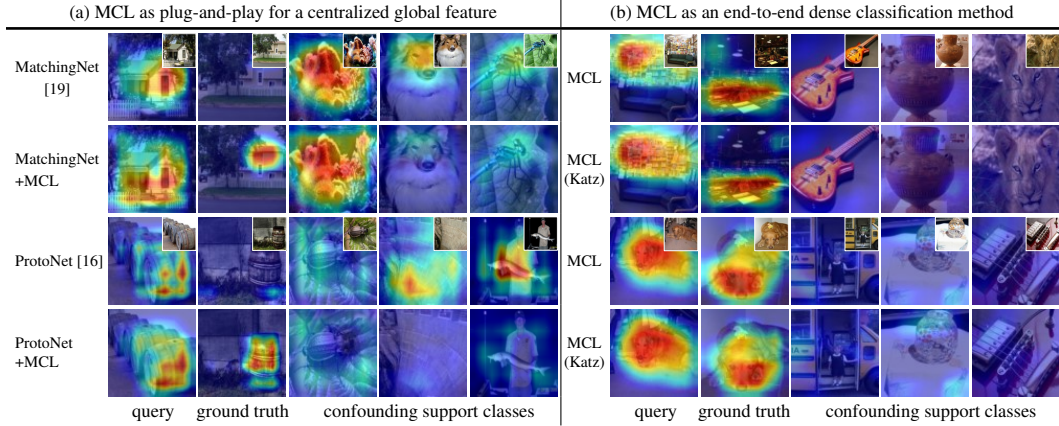


Table 4: Grad-CAM visualizations of query and support images in 4-way 1-shot classifications. The left pane (a) illustrates MCL as plug-and-play on *tieredImageNet*. The right pane (b) illustrates MCL as an end-to-end dense classification method on *miniImageNet*. Images at the second column of each task are from the ground truth while the others are from the confounding support classes.

that, for an extremely small $\alpha \rightarrow 0$, the accuracy of MCL-Katz will be only decided by γ in the one-step query-to-support random walk and the method will degrade to the unidirectional averaged dense classification like [8] where the contributions from paths longer than one just vanished. The performance can be improved by considering the mutual affiliations for an increasing value of α . It can also be observed in Figure 2(a) that the accuracy tends to decline when $\alpha \rightarrow 1$, which indicates it is more reasonable to penalize the contributions of distant nodes in MCL as the affiliations between them are comparably weaker and less reliable than those of short paths.

Long-term v.s. finite short-term features’ accessibility in Markov process. Figure 2(b) shows the ablative results of using short-term features’ accessibility from various finite steps of the Markov process. We see that the performance gains by the long term of random walks gradually saturate for the increasing values of t as contributions from far distant nodes get vanished due to the exponential decreasing of α^t in MCL-Katz. With appropriate α , we see using the long-term features’ accessibility for classifications consistently outperforms those from the finite short-term’s accessibility.

Qualitative visualizations of the feature centralization. We have shown that MCL can serve both as plug-and-play for global feature representations and as a novel end-to-end classification method motivated by the features’ accessibility. To get a deeper understanding of it, we visualize the Grad-CAM [14] of the last convolutional layer in ResNet-12 for both query and support images in Table 4. We see in Table 4(a) that the native global feature based methods fail to identify the most relevant regions of interests in each task that leads to a misclassification (e.g., ProtoNet [16] misclassified the query image to the 4-th classes in the example). By replacing global average pooling with centrality weighted pooling, we see it identifying those regions of interests and removing the confounding areas in predictions. We also visualize the CAM of our end-to-end MCL methods in Table 4(b). It can be seen that the most centralized support features are generally from the ground-truth and are mutually affiliated with the task-relevant objects of the query images. It qualitatively validates the underlying assumption of MCL that support features would be frequently visited in the long term of bidirectional random walks by their mutual affiliations if they shared the same class as the query image.

5 Conclusions

We present a novel dense feature based framework: Mutual Centralized Learning (MCL) to highlight the mutual affiliations of bipartite dense features in FSL. Specifically, we propose a novel bidirectional random walks paradigm and introduce a novel classification criterion by the features’ accessibility in a time-homogeneous Markov process. We demonstrate such accessibility is equivalent to learning a single-mode centrality of an affiliation network and demonstrate its capability to be plugged in existing metric-based methods. Experimental results demonstrate MCL achieves the state-of-the-art on both *miniImageNet* and *tieredImageNet*.

References

- [1] Phillip Bonacich. Factoring and weighting approaches to status scores and clique identification. *Journal of mathematical sociology*, 2(1):113–120, 1972.
- [2] Phillip Bonacich. Simultaneous group and individual centralities. *Social networks*, 13(2):155–168, 1991.
- [3] Stephen P Borgatti and Martin G Everett. Network analysis of 2-mode data. *Social networks*, 19(3):243–269, 1997.
- [4] Wei-Yu Chen, Yen-Cheng Liu, Zsolt Kira, Yu-Chiang Frank Wang, and Jia-Bin Huang. A closer look at few-shot classification. In *International Conference on Learning Representations*, 2019.
- [5] Leo Katz. A new status index derived from sociometric analysis. *Psychometrika*, 18(1):39–43, 1953.
- [6] Kwonjoon Lee, Subhransu Maji, Avinash Ravichandran, and Stefano Soatto. Meta-learning with differentiable convex optimization. In *Proceedings of the IEEE/CVF Conference on Computer Vision and Pattern Recognition*, pages 10657–10665, 2019.
- [7] Wenbin Li, Lei Wang, Jinglin Xu, Jing Huo, Yang Gao, and Jiebo Luo. Revisiting local descriptor based image-to-class measure for few-shot learning. In *Proceedings of the IEEE/CVF Conference on Computer Vision and Pattern Recognition*, pages 7260–7268, 2019.
- [8] Yann Lifchitz, Yannis Avrithis, Sylvaine Picard, and Andrei Bursuc. Dense classification and implanting for few-shot learning. In *Proceedings of the IEEE/CVF Conference on Computer Vision and Pattern Recognition*, pages 9258–9267, 2019.
- [9] Yanbin Liu, Juho Lee, Minseop Park, Saehoon Kim, Eunho Yang, Sung Ju Hwang, and Yi Yang. Learning to propagate labels: Transductive propagation network for few-shot learning. In *International Conference on Learning Representations*, 2019.
- [10] Adam Paszke, Sam Gross, Francisco Massa, Adam Lerer, James Bradbury, Gregory Chanan, Trevor Killeen, Zeming Lin, Natalia Gimelshein, Luca Antiga, Alban Desmaison, Andreas Kopf, Edward Yang, Zachary DeVito, Martin Raison, Alykhan Tejani, Sasank Chilamkurthy, Benoit Steiner, Lu Fang, Junjie Bai, and Soumith Chintala. Pytorch: An imperative style, high-performance deep learning library. In H. Wallach, H. Larochelle, A. Beygelzimer, F. d’Alché-Buc, E. Fox, and R. Garnett, editors, *Advances in Neural Information Processing Systems 32*, pages 8024–8035. Curran Associates, Inc., 2019.
- [11] Oskar Perron. Zur theorie der matrizes. *Mathematische Annalen*, 64(2):248–263, 1907.
- [12] Mengye Ren, Eleni Triantafillou, Sachin Ravi, Jake Snell, Kevin Swersky, Joshua B Tenenbaum, Hugo Larochelle, and Richard S Zemel. Meta-learning for semi-supervised few-shot classification. In *International Conference on Learning Representations*, 2018.
- [13] Ravi Sachin and Laroche Hugo. Optimization as a model for few-shot learning. *ICLR*, 2017.
- [14] Ramprasaath R Selvaraju, Michael Cogswell, Abhishek Das, Ramakrishna Vedantam, Devi Parikh, and Dhruv Batra. Grad-cam: Visual explanations from deep networks via gradient-based localization. In *Proceedings of the IEEE international conference on computer vision*, pages 618–626, 2017.
- [15] Christian Simon, Piotr Koniusz, Richard Nock, and Mehrtash Harandi. Adaptive subspaces for few-shot learning. In *CVPR*, pages 4136–4145, 2020.
- [16] Jake Snell, Kevin Swersky, and Richard Zemel. Prototypical networks for few-shot learning. In *NIPS*, pages 4077–4087, 2017.
- [17] Qianru Sun, Yaoyao Liu, Tat-Seng Chua, and Bernt Schiele. Meta-transfer learning for few-shot learning. In *Proceedings of the IEEE/CVF Conference on Computer Vision and Pattern Recognition*, pages 403–412, 2019.
- [18] Flood Sung, Yongxin Yang, Li Zhang, Tao Xiang, Philip HS Torr, and Timothy M Hospedales. Learning to compare: Relation network for few-shot learning. In *CVPR*, pages 1199–1208, 2018.
- [19] Oriol Vinyals, Charles Blundell, Timothy Lillicrap, Koray Kavukcuoglu, and Daan Wierstra. Matching networks for one shot learning. In *Proceedings of the 30th International Conference on Neural Information Processing Systems*, pages 3637–3645, 2016.
- [20] Chi Zhang, Yujun Cai, Guosheng Lin, and Chunhua Shen. Deepemd: Differentiable earth mover’s distance for few-shot learning. *arXiv e-prints*, pages arXiv–2003, 2020.
- [21] Dengyong Zhou, Olivier Bousquet, Thomas N. Lal, Jason Weston, and Bernhard Schölkopf. Learning with local and global consistency. In *Advances in Neural Information Processing Systems 16*, volume 16, pages 321–328, 2003.

Appendix for Mutual Centralized Learning in Few-shot Classifications

A Algorithm for Episode Loss

Algorithm 1 Episodic Loss for N -way K -shot Mutual Centralized Learning.

Notations:

$\mathcal{C}_{\text{train}}$: the set of training classes.
 $\mathcal{C}_{\text{episode}}$: the set of randomly selected classes in each episode.
 N_Q : the number of selected query examples per class in each episode.
 $\mathcal{D}_{\text{train}}$: the set of training data $\{(x_0, y_0), (x_1, y_1), \dots\}$ where x is an image and y is its label.
 \mathcal{D}_c : the subset of $\mathcal{D}_{\text{train}}$ that belongs to class c
 $\mathcal{Q}_{\text{episode}}$: the set of query data in each episode.
 $\mathcal{S}_{\text{episode}}^c$: the set of support data of class c in each episode.
 \mathbf{q} : the set of dense features of a single query image.
 \mathbf{s}^c : the set of dense features of class c in each episode.
 \mathbf{S} : the set of dense features of all classes in each episode.

Require:

$\text{RANDOMSAMPLE}(\{\cdot\}, k)$: random sampling k elements from set $\{\cdot\}$ without replacement.
 $f_\theta(x)$: function to dense features given the input image x (e.g., feature map from *VanillaFCN*).
 $\mathbb{1}[\cdot]$: indicator function that equals one if its argument is true and zero otherwise

Procedure:

```

1:  $\mathcal{Q}_{\text{episode}} \leftarrow \{\}$ 
2:  $\mathcal{C}_{\text{episode}} \leftarrow \text{RANDOMSAMPLE}(\mathcal{C}_{\text{train}}, N)$                                  $\triangleright$  Select  $N$ -way classes for episode
3: for  $c$  in  $\mathcal{C}_{\text{episode}}$  do
4:    $\mathcal{S}_{\text{episode}}^c \leftarrow \text{RANDOMSAMPLE}(\mathcal{D}_c, K)$                                  $\triangleright$  Select  $K$ -shot support examples per class
5:    $\mathbf{s}^c \leftarrow 0$ 
6:   for  $(x, y) \in \mathcal{S}_{\text{episode}}^c$  do
7:      $\mathbf{s}^c \leftarrow \mathbf{s}^c + f_\theta(x)/K$      $\triangleright$  Average support features from  $K$ -shot images of the same class
8:   end for
9:    $\mathcal{Q}_{\text{episode}} \leftarrow \mathcal{Q}_{\text{episode}} \cup \text{RANDOMSAMPLE}(\mathcal{D}_c \setminus \mathcal{S}_{\text{episode}}^c, N_Q)$   $\triangleright$  Select  $N_Q$  queries per class
10: end for
11:  $\mathbf{S} \leftarrow \bigcup_{c \in \mathcal{C}_{\text{episode}}} \mathbf{s}^c$                                  $\triangleright$  Union support features of different classes within an episode
12:  $\mathcal{L} \leftarrow 0$                                  $\triangleright$  Initialize episodic loss
13: for  $(x, y)$  in  $\mathcal{Q}_{\text{episode}}$  do
14:    $\mathbf{q} \leftarrow f_\theta(x)$ 
15:   Compute matrix  $\Phi_\gamma$ ,  $\Phi_\tau$ , and their normalization matrices  $\mathbf{D}$  and  $\mathbf{W}$  by Eqn.(1, 2)
16:   Construct transition matrix  $\mathbf{P}$  by Eqn.(4)
17:   Compute complete Katz centrality or approximated eigenvector centrality by Eqn.(10, 12)
18:   Compute probability  $\mathbf{Pr}(\tilde{y} = c)$  for class  $c$  by Eqn.(13) for MCL (or Eqn.(11) for MCL-Katz).
19:    $\mathcal{L} \leftarrow \mathcal{L} - \frac{1}{NN_Q} \left[ \sum_{c \in \mathcal{C}_e} \mathbb{1}[y = c] \log \mathbf{Pr}(\tilde{y} = c) \right]$                                  $\triangleright$  Negative log-likelihood loss
20: end for

```

B Proof of Eqn.(5)

Eqn.(5): Given the anti-diagonal Markov transition matrix $\mathbf{P} = \begin{pmatrix} \mathbf{0} & \mathbf{P}_{\mathbf{S}\mathbf{q}} \\ \mathbf{P}_{\mathbf{q}\mathbf{S}} & \mathbf{0} \end{pmatrix}$ that is composed of two column-normalized submatrices $\mathbf{P}_{\mathbf{S}\mathbf{q}}$, $\mathbf{P}_{\mathbf{q}\mathbf{S}}$, the stationary distribution is periodic with equation:

$$\lim_{t \rightarrow \infty} \mathbf{P}^{2t} = \begin{pmatrix} \pi(\mathbf{S})e_{|\mathbf{S}|}^T & \mathbf{0} \\ \mathbf{0} & \pi(\mathbf{q})e_{|\mathbf{q}|}^T \end{pmatrix} \quad \lim_{t \rightarrow \infty} \mathbf{P}^{2t-1} = \begin{pmatrix} \mathbf{0} & \pi(\mathbf{S})e_{|\mathbf{q}|}^T \\ \pi(\mathbf{q})e_{|\mathbf{S}|}^T & \mathbf{0} \end{pmatrix}$$

where $\pi(\mathbf{S})$ is the stationary vector of $\mathbf{P}_{\mathbf{S}\mathbf{q}}\mathbf{P}_{\mathbf{q}\mathbf{S}}$ and $\pi(\mathbf{q})$ is the stationary vector of $\mathbf{P}_{\mathbf{q}\mathbf{S}}\mathbf{P}_{\mathbf{S}\mathbf{q}}$. $e_{|\cdot|}$ denotes a vector of ones with different length indicated by its subscript.

Proof of periodic: Consider the eigenvalue λ of \mathbf{P} with determinant

$$\det(\lambda\mathbf{I} - \mathbf{P}) = \det \begin{pmatrix} \lambda\mathbf{I} & -\mathbf{P}_{\mathbf{S}\mathbf{q}} \\ -\mathbf{P}_{\mathbf{q}\mathbf{S}} & \lambda\mathbf{I} \end{pmatrix} = \det(\lambda^2\mathbf{I} - \mathbf{P}_{\mathbf{S}\mathbf{q}}\mathbf{P}_{\mathbf{q}\mathbf{S}}) \quad (\text{B.1})$$

it can be found that the eigenvalues of \mathbf{P} are the square roots of eigenvalues of $\mathbf{P}_{\mathbf{S}\mathbf{q}}\mathbf{P}_{\mathbf{q}\mathbf{S}}$.

Since the subblocks of $\mathbf{P}_{\mathbf{S}\mathbf{q}}$ and $\mathbf{P}_{\mathbf{q}\mathbf{S}}$ are both column-normalized matrices as defined in Eqn.(1,2), their product is column-stochastic that can be proved by:

$$e_{|\mathbf{S}|}^T \mathbf{P}_{\mathbf{S}\mathbf{q}} \mathbf{P}_{\mathbf{q}\mathbf{S}} = e_{|\mathbf{q}|}^T \mathbf{P}_{\mathbf{q}\mathbf{S}} = e_{|\mathbf{S}|}^T \quad (\text{B.2})$$

We know (by the definition of stochastic matrix) that $\lambda = 1$ is the largest eigenvalue of $\mathbf{P}_{\mathbf{S}\mathbf{q}}\mathbf{P}_{\mathbf{q}\mathbf{S}}$, and its uniqueness is guaranteed since there is no zero entry in both $\mathbf{P}_{\mathbf{S}\mathbf{q}}$ and $\mathbf{P}_{\mathbf{q}\mathbf{S}}$. According to Eqn.(B.1), we get another eigenvalue $\lambda = -1$ for stochastic matrix \mathbf{P} . From the Perron–Frobenius theorem that the period of \mathbf{P} equals to the number of eigenvalue whose absolute value is equal to the spectral radius of \mathbf{P} , we can get its stationary distribution is of period 2.

Proof of stationary distribution for even periods: Consider the even power of matrix \mathbf{P} in extreme

$$\lim_{t \rightarrow \infty} \mathbf{P}^{2t} = \lim_{t \rightarrow \infty} \begin{pmatrix} \mathbf{P}_{\mathbf{S}\mathbf{q}}\mathbf{P}_{\mathbf{q}\mathbf{S}} & \mathbf{0} \\ \mathbf{0} & \mathbf{P}_{\mathbf{q}\mathbf{S}}\mathbf{P}_{\mathbf{S}\mathbf{q}} \end{pmatrix}^t = \begin{pmatrix} \lim_{t \rightarrow \infty} [\mathbf{P}_{\mathbf{S}\mathbf{q}}\mathbf{P}_{\mathbf{q}\mathbf{S}}]^t & \mathbf{0} \\ \mathbf{0} & \lim_{t \rightarrow \infty} [\mathbf{P}_{\mathbf{q}\mathbf{S}}\mathbf{P}_{\mathbf{S}\mathbf{q}}]^t \end{pmatrix} \quad (\text{B.3})$$

We have shown in Eqn.(B.2) that $\mathbf{P}_{\mathbf{S}\mathbf{q}}\mathbf{P}_{\mathbf{q}\mathbf{S}}$ is column-stochastic and use $\pi(\mathbf{S})$ to represent its stationary distribution vector with equation $\lim_{t \rightarrow \infty} [\mathbf{P}_{\mathbf{S}\mathbf{q}}\mathbf{P}_{\mathbf{q}\mathbf{S}}]^t = \pi(\mathbf{S})e_{|\mathbf{S}|}^T$. By analogy, the infinity power of $\mathbf{P}_{\mathbf{q}\mathbf{S}}\mathbf{P}_{\mathbf{S}\mathbf{q}}$ could also reach a similar stationary $\pi(\mathbf{q})$. Thus, we can derive the left part of Eqn.(5) by substituting the two stationary vectors into Eqn.(B.3).

Proof of stationary distribution for odd periods: From the definition, we have

$$\lim_{t \rightarrow \infty} \mathbf{P}^{2t-1} = \lim_{t \rightarrow \infty} \mathbf{P}^{2t+1} = \mathbf{P} \lim_{t \rightarrow \infty} \mathbf{P}^{2t} = \begin{pmatrix} \mathbf{0} & \mathbf{P}_{\mathbf{S}\mathbf{q}}\pi(\mathbf{q})e_{|\mathbf{q}|}^T \\ \mathbf{P}_{\mathbf{q}\mathbf{S}}\pi(\mathbf{S})e_{|\mathbf{S}|}^T & \mathbf{0} \end{pmatrix} \quad (\text{B.4})$$

According to the definition of $\pi(\mathbf{q})$ and $\pi(\mathbf{S})$, we can get

$$\pi(\mathbf{q})e_{|\mathbf{q}|}^T = \lim_{t \rightarrow \infty} [\mathbf{P}_{\mathbf{q}\mathbf{S}}\mathbf{P}_{\mathbf{S}\mathbf{q}}]^t = \mathbf{P}_{\mathbf{q}\mathbf{S}} \left(\lim_{t \rightarrow \infty} [\mathbf{P}_{\mathbf{S}\mathbf{q}}\mathbf{P}_{\mathbf{q}\mathbf{S}}]^t \right) \mathbf{P}_{\mathbf{S}\mathbf{q}} = \mathbf{P}_{\mathbf{q}\mathbf{S}}\pi(\mathbf{S})e_{|\mathbf{S}|}^T \mathbf{P}_{\mathbf{S}\mathbf{q}} \quad (\text{B.5})$$

if we right matrix product of $e_{|\mathbf{q}|}$ on both sides of Eqn.(B.5), we have

$$\pi(\mathbf{q})e_{|\mathbf{q}|}^T e_{|\mathbf{q}|} = \mathbf{P}_{\mathbf{q}\mathbf{S}}\pi(\mathbf{S})e_{|\mathbf{S}|}^T \mathbf{P}_{\mathbf{S}\mathbf{q}} e_{|\mathbf{q}|} \quad (\text{B.6})$$

Since $e_{|\mathbf{q}|}^T e_{|\mathbf{q}|} = |\mathbf{q}|$ and $e_{|\mathbf{S}|}^T \mathbf{P}_{\mathbf{S}\mathbf{q}} e_{|\mathbf{q}|} = \sum_i \sum_j [\mathbf{P}_{\mathbf{S}\mathbf{q}}]_{ij} = |\mathbf{q}|$, Eqn.(B.6) can be simplified by dividing the same scalar $|\mathbf{q}|$ on both sides:

$$\pi(\mathbf{q}) = \mathbf{P}_{\mathbf{q}\mathbf{S}}\pi(\mathbf{S}) \quad (\text{B.7})$$

By analogy, a symmetric equation $\pi(\mathbf{S}) = \mathbf{P}_{\mathbf{S}\mathbf{q}}\pi(\mathbf{q})$ can also be easily proved in the same way from Eqn.(B.5) to Eqn.(B.7). Substituting both $\pi(\mathbf{S}) = \mathbf{P}_{\mathbf{S}\mathbf{q}}\pi(\mathbf{q})$ and $\pi(\mathbf{q}) = \mathbf{P}_{\mathbf{q}\mathbf{S}}\pi(\mathbf{S})$ into Eqn.(B.4) gives the right part of Eqn.(5).

C Proof of Lemma 1.

Proof: We have shown in Appendix B that there exists an eigenvalue $\lambda = 1$ for the column-stochastic matrix \mathbf{P} with equation $\mathbf{P}\mathbf{x} = \mathbf{x}$. If we interpret the transition matrix as an adjacency matrix for the directed bipartite graph, the eigenvector centrality of that graph is \mathbf{x} .

We split the eigenvector \mathbf{x} into $\mathbf{x}_S, \mathbf{x}_q$ for the bipartite vertex set q, S respectively and the single-mode eigenvector centralities of the single vertex set can therefore be formulated by:

$$\hat{\mathbf{x}}_S = \frac{\mathbf{x}_S}{\sum_{s \in S} \mathbf{x}_s} \quad \hat{\mathbf{x}}_q = \frac{\mathbf{x}_q}{\sum_{q \in q} \mathbf{x}_q} \quad (C.1)$$

If we left matrix product \mathbf{P} on both sides of $\mathbf{P}\mathbf{x} = \mathbf{x}$, we will have $\mathbf{P}^2\mathbf{x} = \mathbf{P}(\mathbf{P}\mathbf{x}) = \mathbf{P}\mathbf{x} = \mathbf{x}$. To write it in matrix notation, we have

$$\underbrace{\begin{pmatrix} \mathbf{P}_{Sq}\mathbf{P}_{qS} & \mathbf{0} \\ \mathbf{0} & \mathbf{P}_{qS}\mathbf{P}_{Sq} \end{pmatrix}}_{\mathbf{P}^2} \underbrace{\begin{pmatrix} \mathbf{x}_S \\ \mathbf{x}_q \end{pmatrix}}_{\mathbf{x}} = \underbrace{\begin{pmatrix} \mathbf{x}_S \\ \mathbf{x}_q \end{pmatrix}}_{\mathbf{x}} \quad (C.2)$$

Consider the first row of \mathbf{P}^2 matrix product with \mathbf{x} in Eqn.(C.2), we have $\mathbf{P}_{Sq}\mathbf{P}_{qS}\mathbf{x}_S = \mathbf{x}_S$. Since $\pi(S)$ is the eigenvector of $\mathbf{P}_{Sq}\mathbf{P}_{qS}$ of eigenvalue 1 with probability constraint $\sum_{s \in S} [\pi(S)]_s = 1$, $\pi(S)$ is exactly equivalent to the single-mode eigenvector centrality $\hat{\mathbf{x}}_S$ in Eqn.(C.1).

By analogy, if we consider the matrix product between the second row of \mathbf{P}^2 and \mathbf{x} , we can prove $\pi(q)$ equivalent to the conjugate single-mode eigenvector centrality $\hat{\mathbf{x}}_q$ of the bipartite graph G .

D Supplementary proof of Eqn.(6)

Eqn.(6):

$$\Pr(\tilde{y} = c) = \lim_{t \rightarrow \infty} \frac{\sum_{z \in \mathbf{z}} \mathbb{E} \left[\sum_{k=1}^t \mathbb{1}[X_k \in \mathbf{s}^c] \mid X_0 = z \right]}{\sum_{z \in \mathbf{z}} \mathbb{E} \left[\sum_{k=1}^t \mathbb{1}[X_k \in S] \mid X_0 = z \right]} = \sum_{s \in \mathbf{s}^c} [\pi(S)]_s$$

Let $\Pr(\tilde{y} = c) \triangleq \lim_{t \rightarrow \infty} \Pr(t)$. Since we have shown $\{X_t\}$ is of 2 period in Appendix B, the proof of Eqn.(6) is thus equivalent to prove:

$$\lim_{t \rightarrow \infty} \Pr(2t) = \lim_{t \rightarrow \infty} \Pr(2t-1) = \sum_{s \in \mathbf{s}^c} [\pi(S)]_s \quad (D.1)$$

Proof of even period: $\lim_{t \rightarrow \infty} \Pr(2t) = \sum_{s \in \mathbf{s}^c} [\pi(S)]_s$ (most of which has been shown in Eqn.(6))

From the definition, we have

$$\begin{aligned} \Pr(2t) &= \frac{\frac{1}{|\mathbf{z}|} \sum_{z \in \mathbf{z}} \sum_{k=1}^{2t} \sum_{s \in \mathbf{s}^c} [\mathbf{P}^k]_{sz}}{\frac{1}{|\mathbf{z}|} (|\mathbf{q}|t + |\mathbf{S}|t)} \\ &= \frac{1}{t} \sum_{k=1}^t \left[\frac{1}{|\mathbf{z}|} \sum_{s \in \mathbf{s}^c} \left(\sum_{z \in \mathbf{S}} [\mathbf{P}^{2k}]_{sz} + \sum_{z \in \mathbf{q}} [\mathbf{P}^{2k-1}]_{sz} \right) \right] \end{aligned} \quad (D.2)$$

where $|\mathbf{q}|t$ is the number of visits from particles in \mathbf{q} to support features in \mathbf{S} after $2t$ steps of Markov bidirectional random walk. $|\mathbf{S}|t$ is the number of visits starting from particles in \mathbf{S} to support features in \mathbf{S} . The second equality is derived from the diagonal/anti-diagonal property of $\mathbf{P}^{2k}/\mathbf{P}^{2k-1}$ respectively where the sub-matrices $\mathbf{0}$ are ignored in summation.

Taking it to the extreme, we have

$$\begin{aligned}\lim_{t \rightarrow \infty} \mathbf{Pr}(2t) &= \frac{1}{|\mathbf{z}|} \sum_{s \in \mathbf{s}^c} \left(\sum_{z \in \mathbf{S}} \left[\lim_{t \rightarrow \infty} \mathbf{P}^{2t} \right]_{sz} + \sum_{z \in \mathbf{q}} \left[\lim_{t \rightarrow \infty} \mathbf{P}^{2t-1} \right]_{sz} \right) \\ &= \sum_{s \in \mathbf{s}^c} [\pi(\mathbf{S})]_s\end{aligned}\quad (\text{D.3})$$

where the first equality in Eqn.(D.3) is derived from the *absorbing* of periodic Markov chain and the second equality is from the substitution of Eqn.(5).

$$\text{Proof of odd period: } \lim_{t \rightarrow \infty} \mathbf{Pr}(2t-1) = \sum_{s \in \mathbf{s}^c} [\pi(\mathbf{S})]_s$$

From the definition, we have

$$\begin{aligned}\mathbf{Pr}(2t-1) &= \frac{\frac{1}{|\mathbf{z}|} \sum_{z \in \mathbf{z}} \sum_{k=1}^{2t-1} \sum_{s \in \mathbf{s}^c} [\mathbf{P}^k]_{sz}}{\frac{1}{|\mathbf{z}|} (|\mathbf{q}|t + |\mathbf{S}|(t-1))} \\ &= \frac{1}{|\mathbf{z}|} \frac{1}{t - \frac{|\mathbf{S}|}{|\mathbf{z}|}} \sum_{s \in \mathbf{s}^c} \left[\sum_{z \in \mathbf{q}} \mathbf{P}_{sz} + \sum_{k=2}^t \left(\sum_{z \in \mathbf{S}} [\mathbf{P}^{2k-2}]_{sz} + \sum_{z \in \mathbf{q}} [\mathbf{P}^{2k-1}]_{sz} \right) \right]\end{aligned}\quad (\text{D.4})$$

Take Eqn.(D.4) to the extreme, we have

$$\begin{aligned}\lim_{t \rightarrow \infty} \mathbf{Pr}(2t-1) &= \frac{1}{|\mathbf{z}|} \sum_{s \in \mathbf{s}^c} \left(\sum_{z \in \mathbf{S}} \left[\lim_{t \rightarrow \infty} \mathbf{P}^{2t-2} \right]_{sz} + \sum_{z \in \mathbf{q}} \left[\lim_{t \rightarrow \infty} \mathbf{P}^{2t-1} \right]_{sz} \right) \\ &= \sum_{s \in \mathbf{s}^c} [\pi(\mathbf{S})]_s\end{aligned}\quad (\text{D.5})$$

where $\lim_{t \rightarrow \infty} \frac{1}{t - \frac{|\mathbf{S}|}{|\mathbf{z}|}} \sum_{z \in \mathbf{q}} \mathbf{P}_{sz} = 0$ is ignored when t approaches the infinity.

E Details of Experiment Settings.

E.1 Backbone Network.

Conv-4. It contains four convolutional blocks, each of which consists of a convolutional layer, a batch normalization layer and a Leaky ReLU layer of parameter 0.2. Besides, for each convolutional blocks, an additional 2×2 max-pooling layer is appended, respectively. Given the image of size 84×84 , Conv-4 outputs a feature map of size $5 \times 5 \times 64$.

ResNet-12. We use the same ResNet backbone as in previous literature. Although it is sometimes call ResNet-10 (*e.g.*, in DeepEMD) as they ignore the count of the last fully connected layer, they are indeed the same architecture. The network is composed of four residual blocks, each having three 3×3 convolutional layers with batch normalization and ReLU activation function. Each block is followed by 2×2 max-pooling. The shortcut connections have a convolutional layer to adapt to the right number of channels. The numbers of channels for each block are 64, 160, 320, 640 respectively. Given the image of size 84×84 , ResNet-12 outputs a feature map of size $5 \times 5 \times 640$.

E.2 Dense Feature Extractor.

We compare three kinds of dense feature extractor in our work to demonstrate the effectiveness of our methods. We didn't investigate too much design choices in each extractors, *e.g.*, the size of grids in PyramidGrid, but mainly focus on their native designs as illustrated in Figure 3:

VanillaFCN. VanillaFCN simply treats the feature map output of the fully convolutional network as a set of dense features. For examples, there are 25 64-dimensional dense feature vectors for Conv-4 backbone and 25 640-dimensional dense feature vectors for ResNet-12 backbone.

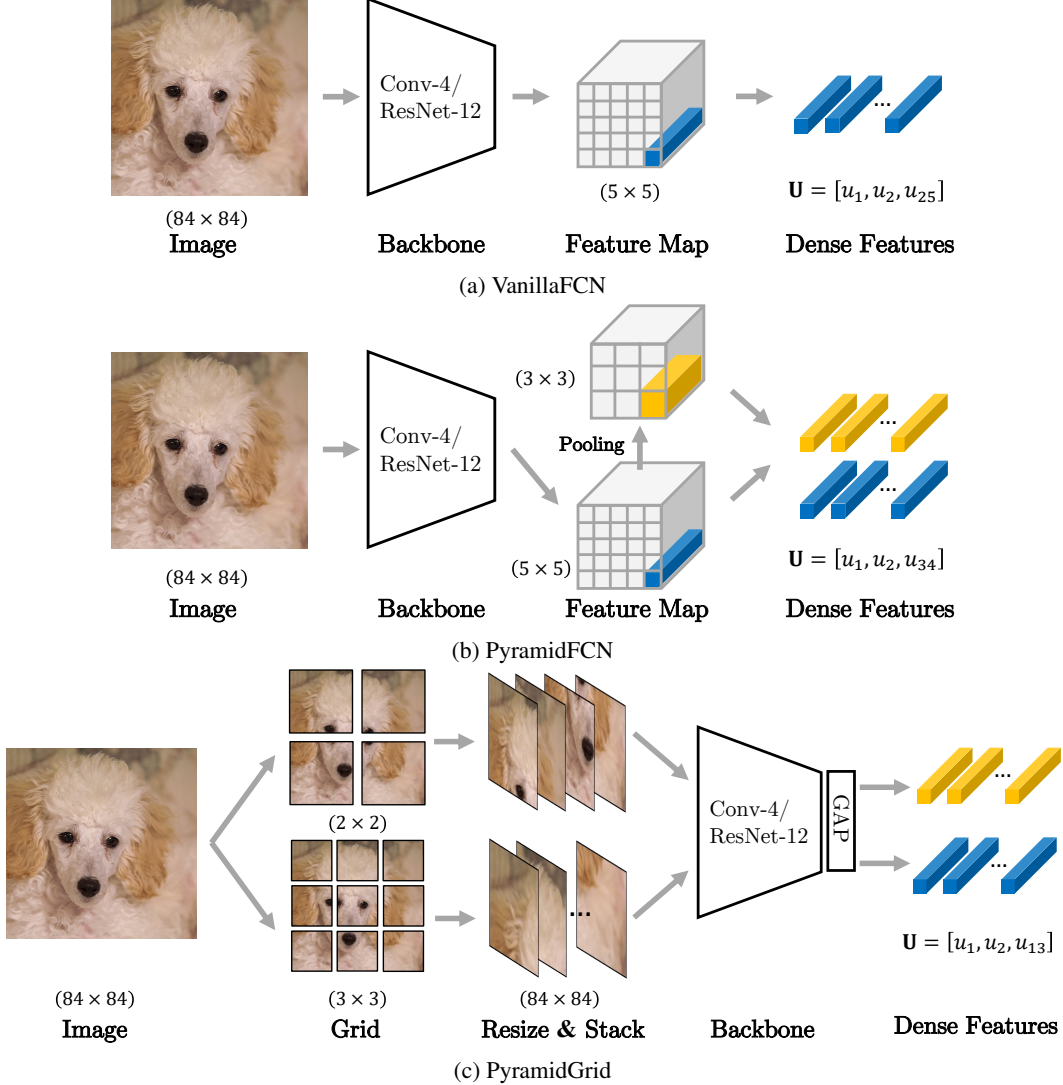


Figure 3: Dense feature extractors to extract local embeddings of the input image. (a) *VanillaFCN* simply treats the feature map output of fully convolutional network as dense features. (b) *PyramidFCN* applies pyramid structures on top of the native feature map to extract dense features of different scales. (c) *PyramidGrid* crops image into grid patches of different scales and encodes each patch to a feature vector with the embedding network. "GAP" indicates a single global average pooling layer.

PyramidFCN. PyramidFCN appends a feature pyramid structure at the end of VanillaFCN to extract local features from multiple image scales. Concretely, we use an extra adaptative average pooling layer of output size 3×3 to obtain 34 ($3 \times 3 + 5 \times 5$) channel-dimensional dense features for each image in our experiment.

PyramidGrid. Grid based extractor first crop the image evenly into an $H \times W$ grid before sending it to the embedding backbone and each image patch in the grid cell is encoded by the network individually. We add a global average pooling (GAP) layer at the end of the backbone so that each image patch will generate a feature vector. The feature vectors generated by all the patches constitute the set of dense features for each image. Like in PyramidFCN, we also adopt an pyramid structure of size $3 \times 3 + 2 \times 2$ in the experiments.

E.3 Training Procedure.

Conv-4. The networks are trained from scratch with gradient descent for the Conv-4 backbone. Specifically, the training is conducted on 30 epochs for both *miniImageNet* and *tieredImageNet*. Each epoch composes 20,000 episodes for training. In each episode, 15 and 10 query images will also be selected from each class for the 1-shot and 5-shot settings, respectively. In other words, for a 5-way 1-shot task, there will be 5 support images and 75 query images in one training episode. To train the Conv-4 model, we adopt Adam algorithm with an initial learning rate 1×10^{-3} and reduce it by 0.1 every 10 epochs.

ResNet-12. The networks are first pre-trained from scratch in a fully supervised manner like previous literature, *i.e.*, minimizing cross-entropy loss on the train split of a dataset. In meta-training stage, we use 30 epochs for *miniImageNet* and 60 epochs for *tieredImageNet* respectively. Each epoch composes 200 episodes for the meta-training. We adopt the SGD with an initial learning rate 5×10^{-4} and reduce it by half every 10 epochs.

For data augmentation in both Conv-4 and ResNet-12, images are resized to 92×92 , randomly cropped to 84×84 and randomly flipped along horizontal axis before used for training.

F Limitations.

The performance of MCL (as well as MCL-Katz) for end-to-end few-shot classifications would be influenced by the hyper-parameters γ, τ as discussed in Section 4.3 and illustrated in Figure 2(a). Like other state-of-the-art metric-based methods in the literature, the parameters are first selected by the pretrained model on the validation set and then fixed during the meta-train/meta-test phases. However, when training from scratch networks like shallow Conv-4, it is hard to pre-select the best combination of parameters. In our experiments on Conv-4, we directly the performance with the selected hyper-parameters γ, τ from ResNet-12.

The attenuation factor α in MCL-Katz also influences the performance. We show in Figure 2(a) that for different combinations of γ and τ , the α for best performances are also different. For example, $\alpha = 0.4$ is the best for $\gamma = 30, \tau = 15$ while $\alpha = 0.7$ is the best for $\gamma = 20, \tau = 20$ on 1-shot *tieredImageNet*. The best α for different dense feature extractor (*e.g.*, *VanillaFCN*, *PyramidFCN*) is also different. We simply report the results of $\alpha = 0.5$ in Table 1 as research of this work is foundational. The results would be higher as shown in Table 5 if we manually selected the best parameters in each task for the engineering purpose, which we thought meaningless in the research.

$(\gamma, \tau) \backslash \alpha$	0.001	0.1	0.2	0.3	0.4	0.5	0.6	0.7	0.8	0.9	0.999
(20, 10)	71.50	71.69	71.74	71.76	71.80	71.81	71.82	71.81	71.83	71.78	71.75
(20, 15)	71.51	71.76	71.80	71.83	71.86	71.86	71.89	71.88	71.89	71.83	71.67
(20, 20)	71.49	71.77	71.84	71.86	71.90	71.88	71.89	71.91	71.89	71.80	71.60
(25, 15)	71.73	71.94	72.01	72.03	72.01	72.01	72.01	72.00	71.98	71.91	71.76
(30, 15)	71.76	71.94	71.94	71.94	71.97	71.92	71.87	71.81	71.81	71.74	71.61

(a) *tieredImageNet* (1-shot) classification accuracy of different parameters.

$(\gamma, \tau) \backslash \alpha$	0.001	0.1	0.2	0.3	0.4	0.5	0.6	0.7	0.8	0.9	0.999
(40, 15)	85.67	86.00	86.10	86.10	86.08	86.07	86.05	86.05	86.06	86.01	85.89
(40, 20)	85.66	86.04	86.11	86.09	86.06	86.02	86.01	86.00	85.99	85.94	85.68
(40, 25)	85.67	86.06	86.12	86.07	86.02	85.99	85.97	85.95	85.93	85.85	85.52
(35, 25)	85.53	85.96	86.05	86.02	85.98	85.97	85.95	85.94	85.90	85.81	85.46
(45, 25)	85.73	86.11	86.14	86.05	86.00	85.97	85.94	85.92	85.88	85.84	85.52

(b) *tieredImageNet* (5-shot) classification accuracy of different parameters.

$(\gamma, \tau) \backslash \alpha$	0.001	0.1	0.2	0.3	0.4	0.5	0.6	0.7	0.8	0.9	0.999
(15, 5)	66.18	66.26	66.27	66.28	66.28	66.29	66.30	66.30	66.30	66.28	66.23
(15, 10)	66.18	66.26	66.27	66.28	66.28	66.27	66.27	66.25	66.21	66.15	66.00
(15, 15)	66.19	66.26	66.26	66.23	66.21	66.19	66.17	66.14	66.09	66.01	65.71
(10, 10)	65.65	65.73	65.74	65.73	65.72	65.72	65.71	65.67	65.63	65.57	65.37
(20, 10)	66.04	66.16	66.17	66.16	66.13	66.11	66.11	66.08	66.04	66.00	65.86

(c) *miniImageNet* (1-shot) classification accuracy of different parameters.

$(\gamma, \tau) \backslash \alpha$	0.001	0.1	0.2	0.3	0.4	0.5	0.6	0.7	0.8	0.9	0.999
(25, 10)	81.49	81.82	81.92	81.94	81.94	81.94	81.93	81.91	81.89	81.87	81.79
(25, 15)	81.49	81.89	81.94	81.94	81.92	81.88	81.85	81.81	81.77	81.73	81.59
(25, 20)	81.49	81.92	81.94	81.91	81.86	81.80	81.74	81.68	81.63	81.59	81.33
(20, 10)	81.35	81.70	81.81	81.87	81.89	81.89	81.89	81.87	81.85	81.83	81.71
(30, 10)	81.50	81.81	81.88	81.89	81.88	81.86	81.84	81.81	81.79	81.77	81.73

(d) *miniImageNet* (5-shot) classification accuracy of different parameters.

Table 5: Detailed statistics on *tieredImageNet* (shown in Figure 2(a)) and *miniImageNet* with ResNet-12 and *VanillaFCN*. We put exact value here for reference. We mark our final choices of parameters (γ, τ) with gray background and the Katz attenuation factor α ($\alpha = 0.999$ reported for MCL, $\alpha = 0.5$ for MCL-Katz) in **bold** font.